


Biomimetic synthesis of vesicular covalent organic frameworks by gemini surfactants for in-situ enzyme cascade immobilization

Received: 3 December 2024

Jin Zhang, You Li, Jiaxuan Li, Lin Zhu & Shangbin Jin  

Accepted: 3 June 2025

Published online: 01 July 2025

 Check for updates

In nature, enzymes in biofilms often lack robustness and chemical functionality. Covalent organic frameworks (COFs) have emerged as a robust platform for enzyme immobilization, but mimicking biofilm structures for in-situ enzyme immobilization remains challenging. Here, we report a biomimetic strategy to synthesize COFs with various morphologies under mild conditions using Gemini surfactants. These surfactants mimic phospholipid bilayers, enabling in-situ enzyme immobilization. Controlled COFs morphologies (vesicular and lamellar) are formed by cationic Gemini surfactants through micelle or reverse micelle regulation. Enzymes with different charges induce distinct COFs morphologies, which in turn affect enzyme activity. This work offers insights into biomimetic morphology control of COFs and their application in enzyme immobilization.

Enzymes serve as nature's precision catalysts, exhibiting high selectivity and excellent catalytic efficiency under relatively mild conditions. They have been employed in a multitude of fields, including biosensing, organic synthesis, biofuels, food industry, fine chemistry, and pharmaceutical chemistry^{1,2}. However, the use of bare enzymes is limited by their vulnerability to environmental changes and the difficulty of recovering them for recycling^{3,4}. In nature, the enzymes in biological systems are immobilized in biofilms in mild conditions, but they usually suffer from insufficient robustness and limited chemical functions. The liposomes that form microcapsules are shown to be able to immobilize the enzymes⁵; however, the self-assembly capsules or vesicles that are built by only surfactants still have shortcomings of insufficient robustness, hindered diffusion, and limited chemical functions. Thus, it is imperative to develop mild and stable biomimetic immobilization systems for enzymes.

Recently, covalent organic frameworks (COFs) are shown as a promising robust immobilizing platform for enzymes^{6–9}, but the study of COFs to mimic the biofilm structure for enzyme immobilization have been rarely reported. Given the structural and functional tunability, as well as extraordinary porosity and crystalline structures, COFs may serve as an effective robust substitute for liposomes in the immobilization of enzymes^{10–12}. Recent advances in COF@enzyme hybrids can be broadly categorized into post-synthetic immobilization

(e.g., physical adsorption^{13–15}, covalent bonding^{16–19}) and in situ encapsulation strategies^{20,21}. Post-synthetic methods, while effective in preserving enzyme activity, often suffer from low loading capacities or enzyme leaching due to weak interfacial interactions²². In contrast, in situ approaches enable direct enzyme encapsulation during COF synthesis, yet harsh reaction conditions (e.g., high temperatures, organic solvents) frequently compromise enzyme integrity¹¹. Recent innovation, such as sacrificial MOF templates^{23,24}, have improved biocompatibility but introduce complexity in template removal or require multi-step processes. Despite these efforts, a critical gap persists: the lack of methodologies to dynamically regulate COFs morphology while maintaining enzyme activity and structural precision, mimicking the hierarchical organization of natural biofilms.

Herein, we develop a bionic strategy for the synthesis of a new type of morphology controllable COFs towards robust enzyme immobilization. The synthesis of the COFs was assisted by the Gemini surfactants under two-phase micelle systems. A series of new Gemini surfactants was designed as phase transfer catalysts to catalyze and induce the self-assembly of COFs for in-situ immobilization of enzymes. Unlike conventional COF-based immobilization methods, our approach leverages the dual roles of cationic Gemini surfactants as both phase-transfer catalysts and structural templates, enabling the formation of vesicular or lamellar COFs under mild aqueous

conditions. By mimicking phospholipid bilayers, these COFs create a biomimetic interface that enhances enzyme stability while facilitating substrate diffusion. By designing tailored geometries through interactions between hydrophilic enzymes and charged surfactants, we revealed that the enzymes induced the micelle transformation in the Gemini surfactant systems, which indicates that the enzymes have participated in the morphological transformation of COFs. The enzymes that are immobilized within the COFs synthesized by Gemini surfactants display higher stabilities and activities than that by monocationic surfactants as well as other immobilization systems. Our biomimetic strategy not only replicates the structural hierarchy of natural biofilms but also introduces dynamic morphology control through enzyme-surfactant interactions, thereby reveals the underlying relationship between morphology and performance. Moreover, the target immobilization of enzymes based on their charge properties can be realized.

Results

Synthesis strategy for morphological COFs

In biological system, the phospholipid bilayer of biofilm represents the fundamental scaffold of biological membranes, providing effective protection for proteins²⁵. The phospholipid bilayer structure may be mimicked by Gemini surfactants via self-assembly, which is based on the unique structure of Gemini surfactants that comprise of two polar headgroups, large hydrophobic tails, and low critical micelle concentration²⁶. Enlightened by the natural phospholipid bilayer structures, it is promising to combine the Gemini surfactant with a robust immobilizer, so as to mimic a “robust biological membrane” and provide a biomimetic system as a new stable enzyme host.

Inspired by the phospholipid bilayer's role in natural biofilms, we hypothesize that Gemini surfactants—with their dual hydrophilic heads and flexible hydrophobic tails—could serve as dynamic templates for COF self-assembly. This approach combines the structural robustness of COFs with the morphological adaptability of biomimetic systems, addressing the limitations of current enzyme immobilization strategies. Along this line, TpPa-COFs were prepared by reacting 1,3,5-triformylphloroglucinol (Tp) with *p*-phenylenediamine (Pa) by the designed Gemini surfactants in aqueous-oil two phases. As shown in Fig. 1a, two surfactants were initially evaluated to synthesize TpPa-COF. As evaluated by powder X-ray diffraction (PXRD) and nitrogen sorption isotherm measurements, the crystallinity and porosity are correlated with the reaction conditions, such as surfactants, solvents and stabilizers. The polymerization employing 4,4'-(ethane-1,2-diyl) bis(1-cetylpyridine-1-ium) bromide (C₁₆Py-2-Py16), and N¹, N²-dihexadecyl-N¹, N²-tetramethylethane-1,2-diaminium bromide (C₁₆-2-16) as surfactants with a concentration of 1 mg mL⁻¹ enabled the quick synthesis of COFs with well-defined morphologies in 10 min at 25 °C. The TpPa-COFs formed in the presence of C₁₆-2-16 exhibited the optimal XRD diffraction pattern (Supplementary Fig. 1a), which consists of a series of clear peaks at 4.7°, 8.2°, 12.7° and 27.2°. The PXRD patterns of these COFs match well with the literature results²⁷, which are assignable to the facets of (100), (110), (120), and (001), respectively.

The FT-IR spectra (Supplementary Fig. 1b) of TpPa-COF (C₁₆-2-16) revealed the disappearance of the carbonyl stretching band of Tp (1639 cm⁻¹) along with a series of new characteristic stretching bands at 1575 and 1240 cm⁻¹, which are originated from the C=C and C=N stretching bands respectively, confirming the formation of β -ketone-amine COF frameworks. Besides the reported oil-in-water (O/W) reaction system²⁸, the water-in-oil (W/O) reaction system can also result in good crystallization and high specific surface areas (Supplementary Figs. 1c, 2c). Furthermore, C₁₆Py-2-Py16 is another alternative phase transfer catalyst, which can synthesize TpPa-COF in both O/W and W/O systems (Supplementary Fig. 2). Meanwhile, the measurements of ¹³C NMR also proved the chemical structures of COF (Supplementary Figs. 1d, 2d).

It was observed that the morphologies of TpPa-COF were markedly influenced by the surfactants. As shown in Fig. 1b, the TpPa-COF (C₁₆-2-16), which is named as *v*-TpPa-COF (where the “*v*” indicates the vesicular), shows a vesicular morphology (Fig. 1c–f, Supplementary Figs. 3, 4). However, TpPa-COF (C₁₆Py-2-Py16), which is named as *l*-TpPa-COF (where the “*l*” indicates the lamellar), exhibits lamellar morphology in both O/W and W/O (Fig. 1g–k, Supplementary Fig. 5, 6). The different morphologies can be attributed to the Critical Packing Parameter (CPP) of the surfactants. It is established that the surfactant can form spherical micelles by self-assembly when CPP < 1/3, bilayer vesicles when 1/2 < CPP < 1, and bilayer lamellar structure when CPP \approx 1^{29,30}. Thus, the surfactant not only interacts with the monomers to enable the rapid polymerization of the COFs, but also functions as a soft template to induce self-assembly and thereby obtain a distinctive morphology.

In addition to the surfactants, the two-phase micelle systems play another critical role in the self-assembly of TpPa-COFs. The solvent affects the solubility of surfactants and monomers on the one hand, and the interfacial tension between water and oil phases on the other hand. Therefore, in the synthesis of *v*-TpPa-COF in the O/W system the vesicle morphology can be obtained only when the organic phase is dichloromethane (Fig. 1c, d). The optimal synthesis of *v*-TpPa-COF in the W/O system requires a careful adjustment of the solvent ratio, whereby the optimal vesicle morphology can be obtained only when the organic phase is *o*-dichlorobenzene/chloroform (ratio = 3: 2) (Supplementary Figs. 7, 8). In the same reaction system, the replacement of the monomer with Pa-CH₃ resulted in the formation of a crystalline COF with vesicle morphology, indicating that this strategy is extendable (Supplementary Figs. 9, 10).

The amphiphilic polymers comprising long chains with hydrophilic and lipophilic groups were employed as the stabilizing agents. Due to their amphiphilic features, the stabilizers can reach into both phases to form the protective layers for droplets, preventing them from merging with each other. It was found that polyvinylpyrrolidone (PVP) and polyvinyl alcohol (PVA) are excellent stabilizers for the high stability of the morphology formation, and thus can result in uniform sizes of vesicles, while the carboxymethyl cellulose is unfavorable for vesicle morphology (Supplementary Fig. 11). On the one hand, *v*-TpPa-COF has a higher specific surface area when PVA is used as a stabilizer in both O/W and W/O systems compared to PVP. On the other hand, PVA can stabilize surfactant micelles, enhancing COF crystallinity^{31,32}. The optimal PVA concentration controls COF growth, prevents aggregation, and ensures high crystallinity. Therefore, PVA is chosen as the stabilizer in this study³³. (Supplementary Figs. 1c, 12). The amount of PVA required for the synthesis of *v*-TpPa-COF was screened to be 1 mg/mL for the O/W system and 5 mg/mL for the W/O system (Supplementary Fig. 13). The addition of PVA did not significantly alter the morphology of the vesicles (Supplementary Figs. 14, 15). Instead, it resulted in the vesicle size being homogeneous, and the vesicle size decreased from 1 μ m to 100 nm; the vesicle size decreased slightly with the increase of PVA (Supplementary Fig. 16). At the optimal PVA concentration, both systems were observed to form uniform and stable emulsions, with an average diameter of approximately 164 nm in O/W and W/O (Supplementary Fig. 17). The surfaces of the PVP and PVA are positively charged, which is the same as the positively charged surface of the droplets. Therefore, the effect of stabilizers could be attributed to the electrostatic repulsion between the stabilizer and the emulsion droplet that enables the emulsion to stabilize. In contrast, the negative charge of carboxymethyl cellulose has the effect of destabilizing the emulsion (Supplementary Fig. 18).

The method reported in this work can also directly control the hydrophilic and hydrophobic states of COFs by varying the different synthetic phase systems, i.e., W/O or O/W. The contact angle test showed that the TpPa-COF prepared under the O/W system is hydrophobic, while the TpPa-COF synthesized under the W/O system

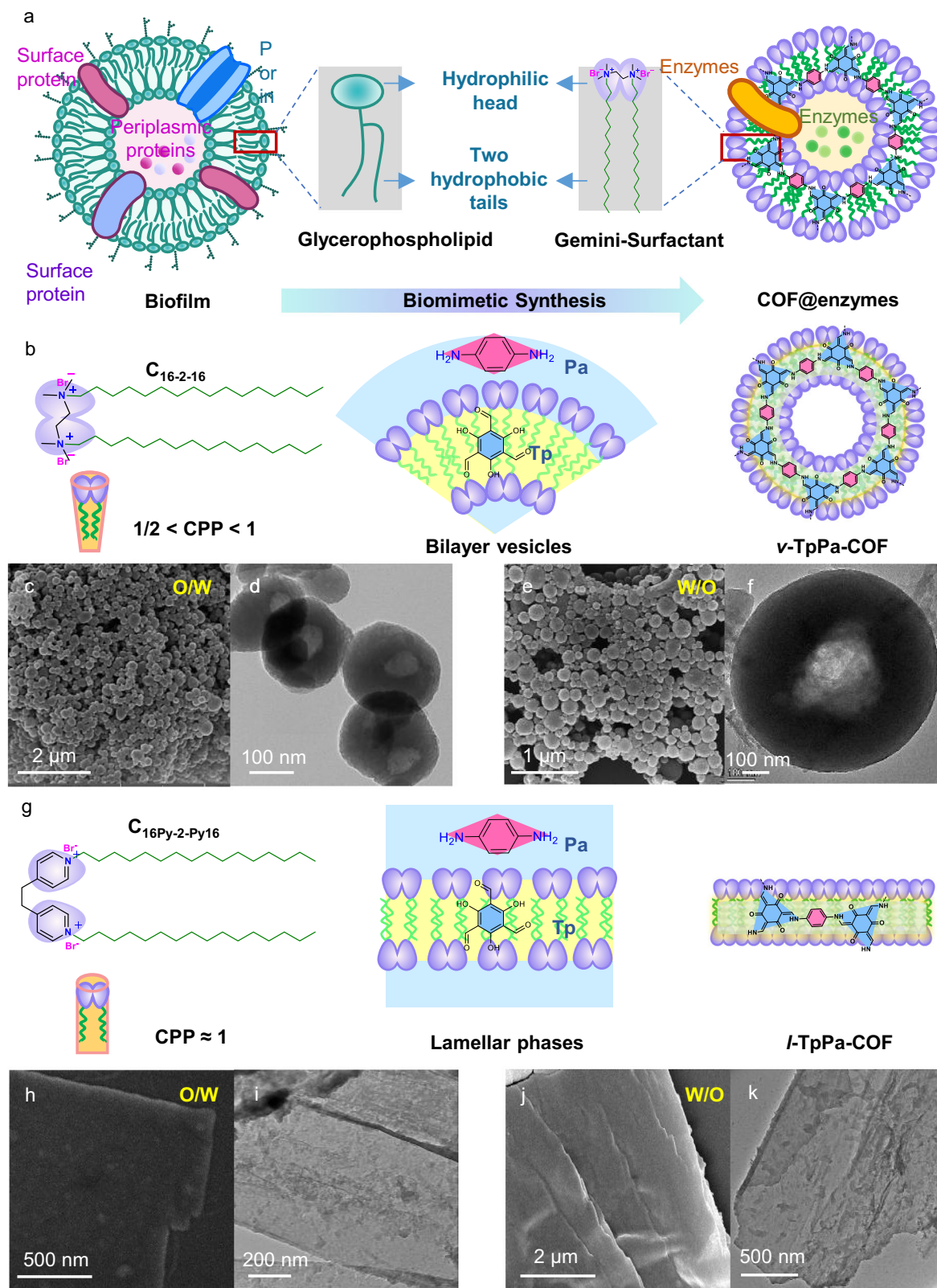


Fig. 1 | Construction of *v*-TpPa-COF and *l*-TpPa-COF. a Illustration of biomimetic synthesis strategy. **b** The synthesis of vesicular *v*-TpPa-COF by the Gemini surfactant $C_{16-2-16}$; **(c)**, SEM image and **(d)**, TEM image of *v*-TpPa-COF(O/W). **e** SEM image

and **(f)**, TEM image of *v*-TpPa-COF(W/O). **g** The synthesis of lamellar *l*-TpPa-COF by the surfactant $C_{16Py-2-Py16}$. **h** SEM image and **(i)**, TEM image of *l*-TpPa-COF(O/W). **j** SEM image and **(k)**, TEM image of *l*-TpPa-COF(W/O).

displayed hydrophilic properties (Supplementary Fig. 19). The reason for this phenomenon can be due to that, the self-assembly of COFs monomers in the oil-in-water system is mainly induced by the lipophilic segment of the surfactant, and the removal of the surfactant makes the outer surface of the COFs exhibit lipophilic characteristics. On the contrary, in the water-in-oil system, the self-assembly of COFs monomers is primarily driven by the hydrophilic segment of the surfactant, resulting in a hydrophilic outer surface after the removal of the surfactant. In addition, as the oil-to-water ratio increased from 5:2 to 60:2, the shell thickness of the COFs vesicles gradually decreased from ~105 nm to ~60 nm (Supplementary Fig. 20).

In-situ enzyme immobilization strategy in ν -TpPa-COF

After establishment of the synthesis of COFs with desired morphologies, the ν -TpPa-COF with vesicular morphology was employed to mimic the cell membrane for the immobilization of enzymes. The glucose oxidase (GOx) and horseradish peroxidase (HRP) were used as enzymes for the in-situ encapsulation. The experiments showed that the enzymes can be immobilized in both the oil-in-water and water-in-oil systems. Notably, the immobilization can be quickly achieved via a one-pot approach by stirring the precursors for 10 min at room temperature. The loading of enzymes in GOx@ ν -TpPa-COF(O/W), GOx@ ν -TpPa-COF(W/O), HRP@ ν -TpPa-COF(O/W), HRP@ ν -TpPa-COF(W/O) were estimated to be 4.6, 5.5, 1.3, and 2.1 wt%, respectively, as determined by thermal gravimetric analysis (Supplementary Fig. 21). Nitrogen adsorption tests (Supplementary Fig. 22) revealed that the BET specific surface areas of the enzyme-loaded COFs were smaller than those of unloaded hybrids, which can be attributed to the occupation of the enzyme in COFs. PXRD measurements showed that the ν -TpPa-COF after encapsulation of both enzymes in the two-phase systems retained the crystalline structures (Supplementary Fig. 23), suggesting that the crystallization proceeded smoothly in the presence of the enzymes.

FT-IR analysis (Supplementary Fig. 24) showed that GOx and HRP have less adverse effect on the condensation reaction within the ν -TpPa-COF precursors, and the FT-IR spectra of four enzyme@ ν -TpPa-COFs showed the characteristic amide band (1700–1600 cm^{-1}), which indicates the successful immobilization of two enzymes in ν -TpPa-COF. Compared with the bare GOx and HRP, the above four enzyme@ ν -TpPa-COFs samples exhibited a red-shift at amide I band regions, suggesting the hydrogen-bonding interactions between ν -TpPa-COF and enzymes³⁴. Furthermore, the contact angle tests demonstrate that the four enzyme@ ν -TpPa-COFs exhibit hydrophilic properties. The GOx@ ν -TpPa-COF(W/O) and HRP@ ν -TpPa-COF(W/O) display better hydrophilicity as compared to the GOx@ ν -TpPa-COF(O/W) and HRP@ ν -TpPa-COF(O/W) (Supplementary Fig. 25). These results clearly indicate that the enzymes are effectively immobilized into the resulting COFs.

Subsequently, we investigated the morphologies of COFs and enzymes after the immobilization. Notably, the SEM and TEM images show that GOx@ ν -TpPa-COF(O/W) displays a worm-like morphology with size around 4 μm (Fig. 2a–c, Supplementary Fig. 26), while GOx@ ν -TpPa-COF(W/O) exhibits a spherical morphology with size around 200 nm (Fig. 2c–f, Supplementary Fig. 27). These morphologies are evidently distinct from the original vesicular morphology of ν -TpPa-COF(O/W) and ν -TpPa-COF(W/O), indicating the morphologies of COFs are markedly influenced by the enzymes. Furthermore, the immobilization of enzymes resulted in alterations to the dimensions of the COFs. The size of GOx@ ν -TpPa-COF(O/W) is larger than the size of ν -TpPa-COF(O/W), and GOx@ ν -TpPa-COF(W/O) is slightly larger than the size of ν -TpPa-COF(W/O). In comparison to GOx, HRP exerts disparate effects on the morphologies of COFs. As evidenced by the SEM and TEM images, HRP@ ν -TpPa-COF retained the original vesicular morphologies in both O/W and W/O systems (Fig. 2g–i, Supplementary Fig. 28, 29). But the sizes of HRP@ ν -TpPa-COF(O/W) (around 122 nm)

and HRP@ ν -TpPa-COF(W/O) (around 68 nm) (Fig. 2i, l) are smaller than the non-immobilized ν -TpPa-COFs. GOx@ ν -TpPa-COF maintains the lamellar morphology in both O/W and W/O systems. In sharp contrast, the e -TpPa-COF(O/W) synthesized using our previously reported mono-cationic surfactant (CPB), only exhibited an irregular spherical morphology after in-situ encapsulating the enzyme. The difference in morphologies indicates the Gemini surfactant is critical for the formation of stable morphologies in the synthesis of ν -TpPa-COF (Supplementary Fig. 30). According to the above results, we conclude that both the enzymes and Gemini surfactants play important roles in inducing the morphology transformation in both O/W and W/O systems.

It was further observed that the morphologies of the resulting enzymes@ ν -TpPa-COF have a strong correlation with the charges of the enzymes and surfactants³⁵. It is noteworthy that both surfactants and enzymes are charged as confirmed by the zeta potential test (Supplementary Fig. 31). It can be observed that the surfactant C₁₆₋₂₋₁₆ which has two positive head groups is positively charged. The GOx shows negatively charged, which is contrary to the surfactant C₁₆₋₂₋₁₆ and the stabilizer PVA. When the enzyme meets with the surfactant in the oil-water interface, the negatively charged GOx tends to attract with the positive head of C₁₆₋₂₋₁₆. The charge interaction between them would induce the surfactant to adjust self-assembly. As the proposed process shown in Fig. 3a, the surfactant and GOx together can induce the COF monomers to assemble into worm-like and spherical morphologies in the O/W and W/O systems, respectively. This speculation can be intuitively proved by CLSM (Fig. 3b–j). When the GOx is stained with RGB dyes, it results in green coloration of RGB-GOx, and red coloration of ν -TpPa-COF, respectively. It is revealed that the GOx can be evenly distributed in the outer layer of worm-like GOx@ ν -TpPa-COF(O/W) (Fig. 3b–d) and spherical GOx@ ν -TpPa-COF(W/O) (Fig. 3e–j), respectively.

The negatively charged HRP exhibits the same charges as the surfactant and stabilizer (Supplementary Fig. 31). Thus, in the assembly process of HRP@ ν -TpPa-COF in both W/O and O/W systems, the repulsive force between the same charged HRP and C₁₆₋₂₋₁₆, enables the HRP to mainly stay in the aqueous phase. As depicted in Fig. 3h, the self-assembly process was proposed. In the O/W system, due to charge repulsion with micelles, HRP that was dispersed in the aqueous phase is difficult to immobilize in COFs. Thus, only a small amount of HRP stayed outside of ν -TpPa-COF via hydrogen-bonding interaction. In the W/O system, the surfactant self-assembles into reversed micelles, which directly encapsulate the dissolved HRP in the oil phase, and eventually enable the self-assembly to form vesicles. As shown in the images by CLSM, the HRP were stained with RGB dyes, resulting in the blue coloration of AF405-HRP. The images of CLSM demonstrate that HRP is predominantly distributed along the periphery of ν -TpPa-COF in W/O system (Fig. 3i–k), whereas the HRP is primarily present within the vesicles in O/W system (Fig. 3l–n).

Bioactivities of encapsulated enzyme cascade in COFs

The performance of enzyme-immobilized COFs is critically influenced by their morphological features, which govern enzyme loading efficiency, substrate accessibility, structural stability, and catalytic activity. Following the successful establishment of the biomimetic immobilization strategy, the bioactivities of the encapsulated enzymes were subsequently evaluated through the use of UV-Vis spectroscopy. Comparing the activities of enzyme@COFs synthesized under different two-phase conditions (Fig. 4a), it is found that the GOx@ ν -TpPa-COF(O/W) exhibited higher activity than the GOx@ ν -TpPa-COF(W/O), whereas HRP@ ν -TpPa-COF(W/O) displayed higher activity than the HRP@ ν -TpPa-COF(O/W). This can be attributed to the fact that the charge of the enzyme affects its immobilization location. For instance, negatively charged GOx is immobilized on the outer side in both GOx@ ν -TpPa-COF(O/W) and GOx@ ν -TpPa-COF(W/O) (Fig. 3b–g),

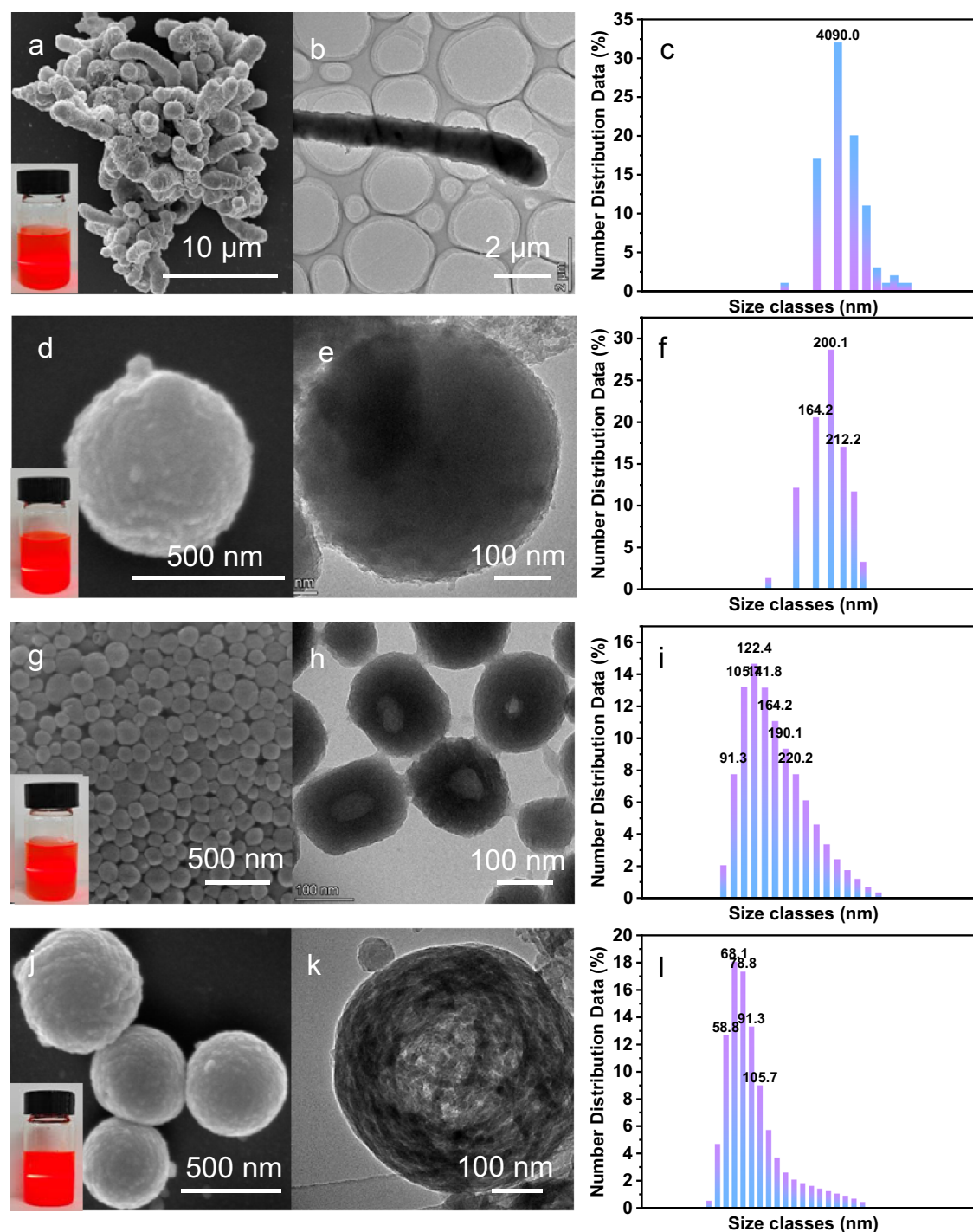


Fig. 2 | Morphologies of enzymes@*v*-TpPa-COF. **a** SEM image, **(b)**, TEM image and **(c)**, the average size of GOx@*v*-TpPa-COF(O/W) (the insert picture is the synthesized COFs emulsion diluted in water). **d** SEM image, **(e)**, TEM image and **(f)**, the

average size of GOx@*v*-TpPa-COF(W/O). **g** SEM image, **h** TEM image and **(i)**, the average size of HRP@*v*-TpPa-COF(O/W). **j** SEM image, **(k)**, TEM image and **(l)**, the average size of HRP@*v*-TpPa-COF(W/O).

allowing free diffusion of the substrate. GOx@*v*-TpPa-COF(O/W) has a higher specific surface area (Supplementary Fig. 22a), which facilitates easier contact between the enzyme and the substrate, thus resulting in higher relative activity. In contrast, positively charged HRP is rarely immobilized in the HRP@*v*-TpPa-COF(O/W) (Fig. 3i–k) but is encapsulated within the vesicles in the HRP@*v*-TpPa-COF(W/O) (Fig. 3l–n). HRP@*v*-TpPa-COF(W/O) also has a higher specific surface area (Supplementary Fig. 22b), leading to higher relative activity. In contrast, the pristine *v*-TpPa-COF exhibits negligible activity, confirming that the catalytic function of the immobilized enzyme@COFs exclusively

originates from the enzyme themselves. A further comparison of the activities of enzyme@COFs synthesized using different surfactants is presented in Fig. 4b. It is shown that the GOx@*v*-TpPa-COF(O/W) exhibited the highest activity within the series. Both the GOx@*v*-TpPa-COF and GOx@*l*-TpPa-COF that are synthesized in O/W and W/O systems, exhibited higher activities than the GOx@*e*-TpPa-COF. These results further prove that the vesicular structure (*v*-TpPa-COF) provides a dual confinement effect for enzyme-substrate interactions due to its porous shell and internal cavity: the shell protects the enzyme from environmental disturbances, while the cavity allows free

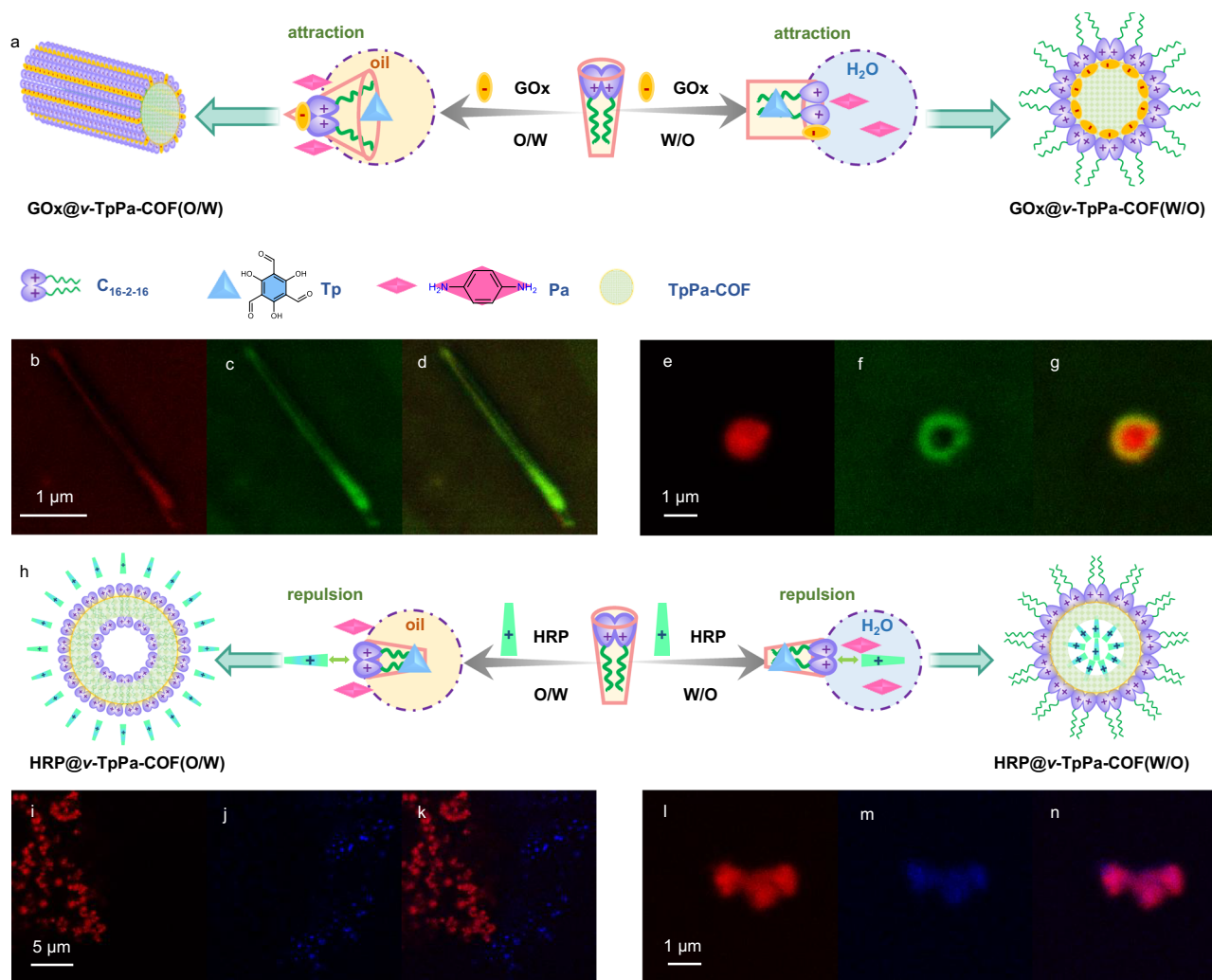


Fig. 3 | Illustration of enzyme induced morphology transformation.

a Illustration of GOx induced morphology transformation of *v*-TpPa-COF; **(b–d)**, CLSM images of GOx@*v*-TpPa-COF(O/W) and **(e–g)**, CLSM images of GOx@*v*-TpPa-

COF(W/O). **h** Illustration of HRP induced morphology transformation of *v*-TpPa-COF. **i–k** CLSM images of HRP@*v*-TpPa-COF(O/W). **l–n** CLSM images of HRP@*v*-TpPa-COF(W/O).

diffusion of the substrate. In contrast, the dense interlayer spacing of the lamellar structure (*l*-TpPa-COF) may restrict substrate mass transfer, leading to reduced activity.

To further investigate the impact of enzyme loading on the COF self-assembly process. We have explored the effects of varying enzyme loading on the morphology and activity of GOx@*v*-TpPa-COF(O/W), GOx@*v*-TpPa-COF(W/O), HRP@*v*-TpPa-COF(O/W), and HRP@*v*-TpPa-COF(W/O). For GOx@*v*-TpPa-COF(O/W), the worm-like morphology was maintained even as the loading of GOx increased (Supplementary Fig. 32). Meanwhile, the enzyme activity significantly rose with higher GOx loading, indicating that the worm-like morphology can accommodate a higher enzyme loading, thereby achieving higher relative activity (Supplementary Fig. 33). In the case of GOx@*v*-TpPa-COF(W/O), the vesicular structure remained intact up to a GOx loading of 12 mg. However, beyond this point, the vesicles ruptured (Supplementary Fig. 34). Correspondingly, the enzyme activity peaked at 12 mg of GOx loading and then decreased due to vesicle rupture (Supplementary Fig. 35), highlighting that it is necessary maintaining vesicle integrity for preserving the activity of immobilized enzymes. Regarding HRP@*v*-TpPa-COF(O/W) (Supplementary Fig. 36), the vesicular structure transformed into spindle-like and rod-like shapes as the HRP loading increased (Supplementary Fig. 37). This morphological change may be attributed to the electrostatic shielding effect of HRP, which altered the vesicle morphology. The rod-like morphology can

accommodate a higher enzyme loading, thereby achieving higher relative activity (Supplementary Fig. 38). For HRP@*v*-TpPa-COF(W/O), the spherical vesicle structure was maintained, but the surface became less smooth as the HRP loading increased (Supplementary Fig. 39). The enzyme activity peaked at 12 mg of HRP loading and then decreased. This decline was likely due to the reduced immobilization efficiency of the enzyme. When the amount of HRP is excessive, it may exceed the immobilization capacity of the *v*-TpPa-COF(W/O). Some HRP molecules may not bind well with the *v*-TpPa-COF(W/O), or the binding may not be strong enough, resulting in decreased enzyme immobilization efficiency. These loosely bound enzymes may detach or denature and become inactive during the reaction process, thereby affecting the overall enzyme activity³⁶. While higher enzyme loadings can increase activity, they can also lead to morphological changes and potential instability. Optimizing enzyme loading is crucial to maintain the desired morphology and maximize activity.

To investigate the influence of GOx@*v*-TpPa-COF(W/O) shell thickness on enzyme activity, we adjusted the oil-water ratio in the W/O system. As the oil-to-water ratio increased from 5:2 to 60:2, the shell thickness of the *v*-TpPa-COF(W/O) vesicles decreased. The highest relative enzyme activity was achieved at a shell thickness of approximately 100 nm (oil-water ratio of 15:2) (Supplementary Fig. 40). At a ratio of 30:2, vesicles began to show surface perforations, and at 60:2, the thin shell made it difficult to form complete vesicles. Further

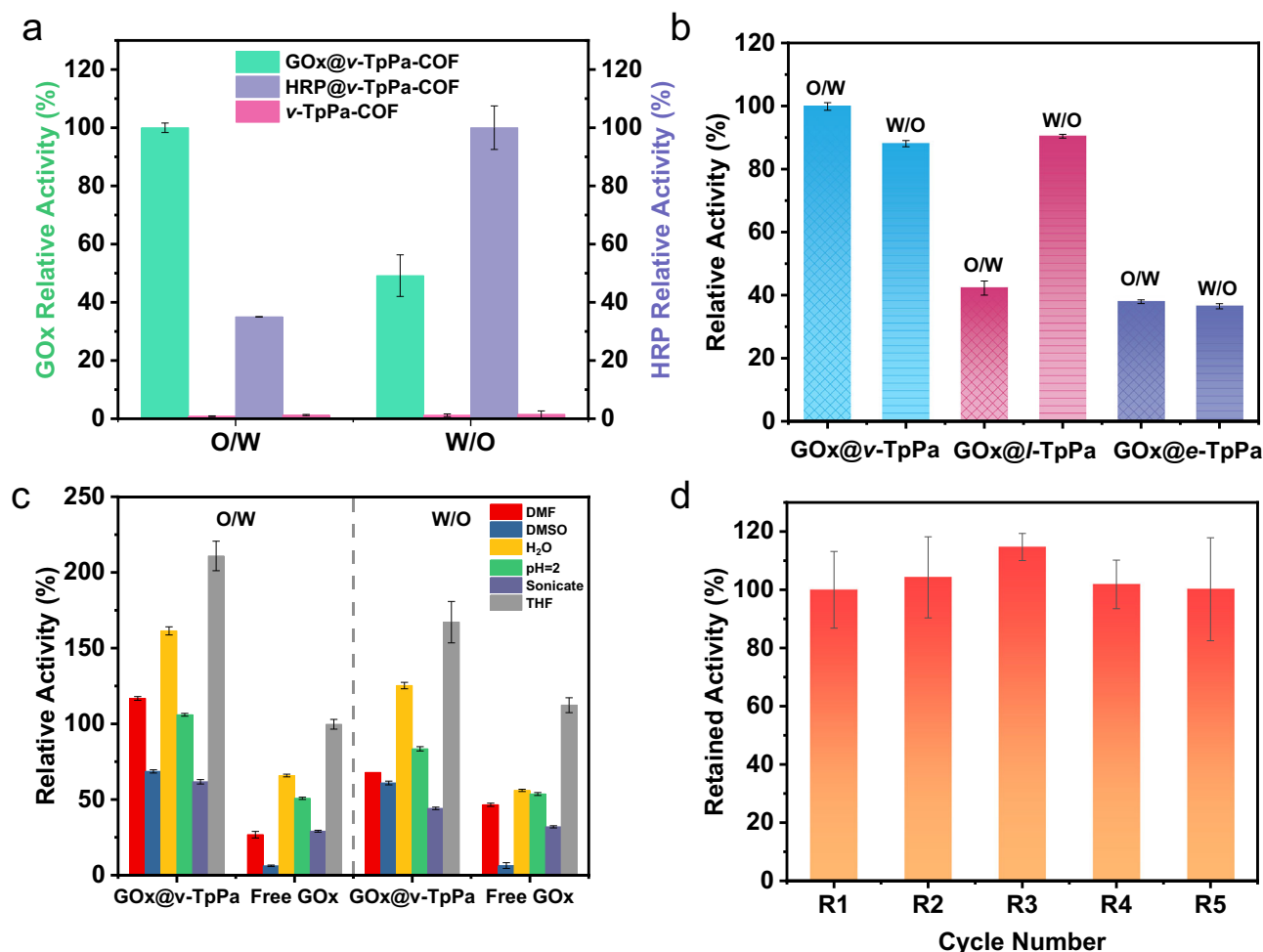


Fig. 4 | Results of the activity and stability for fabricating enzyme@*v*-TpPa-COF. **a** Relative activities of *v*-TpPa-COF(O/W), *v*-TpPa-COF(W/O), GOx@*v*-TpPa-COF(O/W), GOx@*v*-TpPa-COF(W/O), HRP@*v*-TpPa-COF(O/W) and HRP@*v*-TpPa-COF(W/O). **b** Relative activities of GOx@*v*-TpPa-COF, GOx@*l*-TpPa-COF and GOx@*e*-TpPa-COF prepared in O/W and W/O, respectively. **c** Relative activities of

GOx@*v*-TpPa-COF(O/W), GOx@*v*-TpPa-COF(W/O) and free GOx after treatments in DMF, DMSO, H₂O, acid solution, sonication and THF. **d** Recyclability of GOx@*v*-TpPa-COF(O/W). Error bars represent the standard deviation (SD) of three independent experiments.

reduction in shell thickness led to decreased activity, likely due to perforations causing enzyme leakage (Supplementary Fig. 41). This suggests that maintaining the integrity of the vesicular structure is necessary for ensuring high activity.

To explore the impact of GOx@*v*-TpPa-COF(W/O) quantity on enzyme activity, we varied the monomer concentration in the W/O system. Monomer concentrations tested were 120%, 100%, 80%, 60%, 40%, and 20% of the original concentration, all maintaining vesicular morphology. Upon immobilizing GOx, we observed that as the COF quantity decreased, the vesicle volume increased. The highest relative enzyme activity was achieved at a monomer concentration of 60%, where the vesicle volume was largest (Supplementary Fig. 43). Further reduction in monomer concentration led to vesicle rupture and decreased enzyme activity (Supplementary Fig. 44). Reducing the amount of COF has the same effect as previously mentioned increasing the loading of GOx; the rupture of vesicles leads to enzyme leakage, thereby causing a decrease in activity.

To comprehensively evaluate our biomimetic immobilization strategy, we investigated the catalytic activity and stability of enzyme@COF composites under various conditions. The results demonstrate that immobilized enzymes within COFs significantly outperform free enzymes in terms of both activity and stability. Specifically, both GOx@*v*-TpPa-COF(O/W) and GOx@*v*-TpPa-COF(W/O) demonstrate

superior activity in comparison to free enzymes (Fig. 4c), which indicates that *v*-TpPa-COF can provide an excellent protection for GOx. By examining the activities of HRP@*v*-TpPa-COF in different solvents, it was found that HRP@*v*-TpPa-COF(W/O) maintained a better catalytic activity in organic solvents, but the HRP@*v*-TpPa-COF(O/W) was not significantly active (Supplementary Fig. 45). This indicates that the *v*-TpPa-COF can effectively immobilize and protect HRP in the W/O system (Fig. 3h–j). Conversely, a significant amount of HRP is free from *v*-TpPa-COF in the O/W system during self-assembly, making the HRP difficult to be protected (Fig. 3k–m). Additionally, GOx@*v*-TpPa-COF(O/W) maintained higher activity across different pH levels, with the highest relative activity at pH 5. In contrast, free GOx showed significant activity loss under acidic and alkaline conditions (Supplementary Fig. 46). Long-term stability assessments further validated the COFs protective effects. Over 35-day storage, the activity of GOx@*v*-TpPa-COF(O/W) decreased by 27.3%, in contrast, the activity of free GOx decreased by 40.3% over the same period (Supplementary Fig. 47). This underscores the significant protective role of the COF structure in maintaining enzyme activity over extended periods.

Moreover, GOx@*v*-TpPa-COF(O/W) exhibited excellent stability, retaining 99.9% of its initial activity after five cycles (Fig. 4d), compared to only 9.1% for free GOx. Similarly, HRP@*v*-TpPa-COF(O/W) retained 69.8% of its initial activity, while free HRP retained just 6.6%

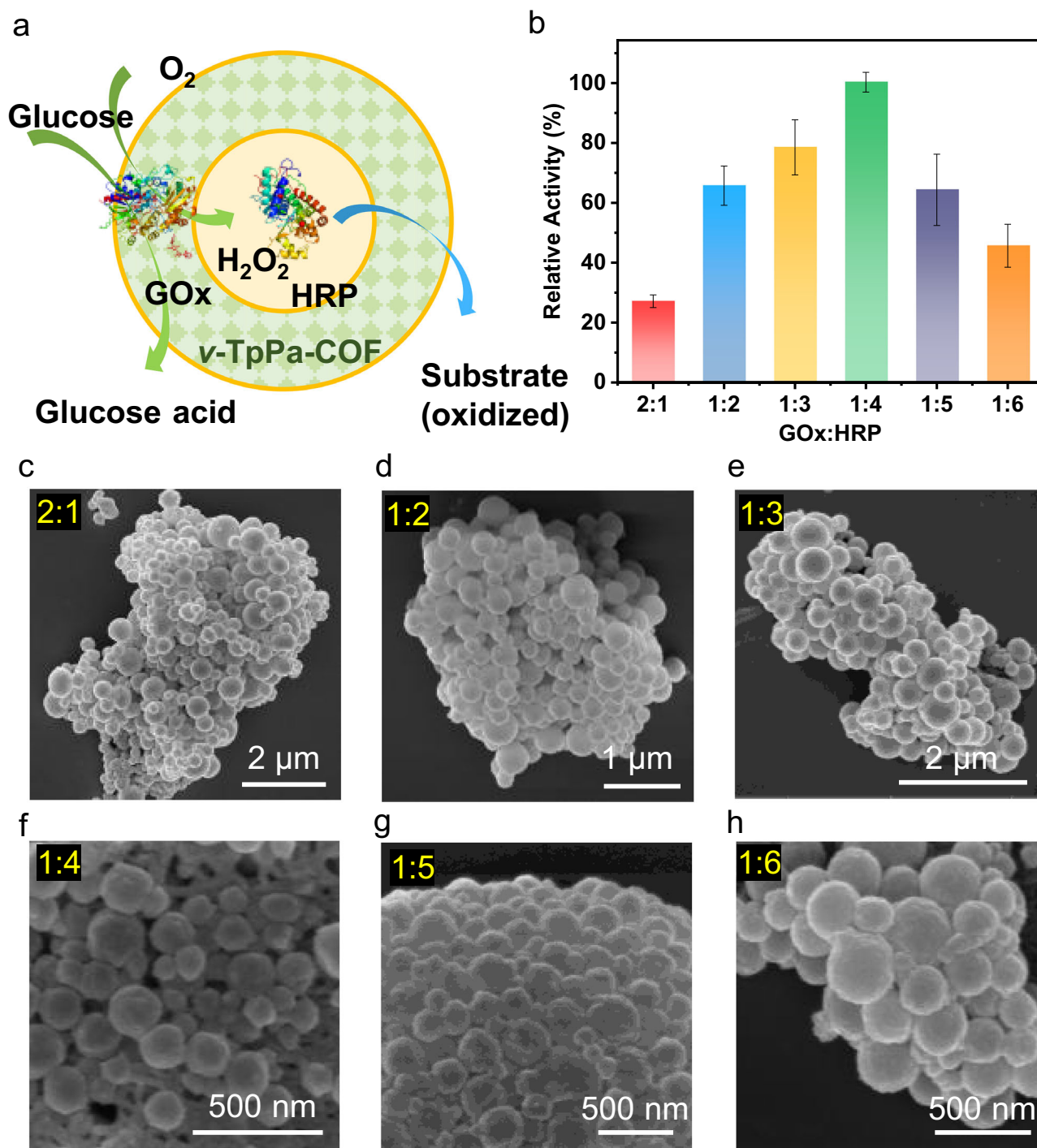


Fig. 5 | Activity and morphology of dual enzyme catalytic cascade. **a** Illustration of dual enzyme catalytic cascade. The structure of GOx (PDB ID: 1CF3) and HRP (PDB ID: 1HCH) was obtained from the Protein Data Bank (RCSB PDB)^{38,39}. **b** Relative activities of with the variation in the ratio of the two enzymes. Error bars represent

the SD of three independent experiments. SEM images of GOx&HRP@v-TpPa-COF(W/O) with the change in the ratio of GOx: HRP, **c** 2:1, **d** 1:2, **e** 1:3, **f** 1:4, **g** 1:5 and **(h)** 1:6.

(Supplementary Fig. 48). The enzyme activity of GOx@v-TpPa-COF(O/W) initially increases due to effective particle dispersion and enhanced mass transfer from stirring, but later decreases due to cumulative material loss from repeated centrifugation. Moreover, after enzyme catalysis, the original morphology was still maintained (Supplementary Fig. 49), and the XRD patterns confirm the preservation of the material's crystalline structure (Supplementary Fig. 50). These findings highlight the superior stability and activity retention of immobilized enzymes, particularly in the O/W system. The leakage rates for GOx@v-

TpPa-COF(O/W), GOx@v-TpPa-COF(W/O), HRP@v-TpPa-COF(O/W), and HRP@v-TpPa-COF(W/O) are estimated to be 8.9%, 15.4%, 8.3%, and 12.4%, respectively (Supplementary Fig. 51). These low leakage rates indicate that the COF structure effectively retains the immobilized enzymes. Kinetic analysis revealed that GOx@v-TpPa(O/W) has a higher maximum reaction rate (v_{max}) of $0.028 \mu\text{mol L}^{-1}\text{s}^{-1}$ compared to free GOx ($0.017 \mu\text{mol L}^{-1}\text{s}^{-1}$) (Supplementary Fig. 52), indicating enhanced catalytic efficiency due to immobilization. Moreover, by the comparison of the immobilization strategies of COFs and MOFs

reported in the literature, the enzyme@COFs in the present work show superior activities to them, highlighting the advantages of this biomimetic immobilization strategy^{34,37} (Supplementary Fig. 53).

In living organisms, biofilms provide attachment sites for diverse enzymes of life activities. To further mimic the enzyme-loaded state of biological membranes, the biomimetic immobilization strategy was utilized to encapsulate dual enzymes (GOx and HRP) in COFs to form a biomimetic catalytic cascade (Fig. 5a). FT-IR and PXRD showed that GOx and HRP could be immobilized into *v*-TpPa-COF in the W/O system and formed a GOx&HRP@*v*-TpPa-COF(W/O) hybrid (Supplementary Fig. 54). SEM images showed that the morphologies can be retained in W/O system, despite the ratios of the dual enzymes are varied (Fig. 5c–h, Supplementary Fig. 55). We performed using CLSM to visualize the spatial distribution of both enzymes when co-immobilized. When GOx and HRP were co-immobilized in the W/O system, the resulting GOx&HRP@*v*-TpPa-COF(W/O) exhibited a solid spherical morphology. The CLSM images revealed that both enzymes were successfully immobilized within the solid spheres (Supplementary Fig. 56). This observation indicates that, in the presence of both enzymes, the self-assembly process of the COFs leads to a more compact and dense structure, encapsulating both GOx and HRP within the same vesicle. When both enzymes are present simultaneously during the self-assembly process, the combined effects of their interactions with the surfactant and the COF monomers lead to a more complex structural arrangement. The formation of solid spheres suggests that the two enzymes are co-localized within the same structure, likely due to the cooperative effects of their charge distributions and the self-assembly dynamics of the COFs.

Optimization of the enzyme activities by varying the ratio of two enzymes showed that the enzyme activities at first increased and then decreased since the gradual variation of GOx/HRP ratios (Fig. 5b). The highest enzyme activity was found at the ratio of GOx/HRP = 1/4, in which the H₂O₂ produced by GOx-catalyzed glucose catabolism can be completely consumed by HRP. When the GOx was in excess, HRP became the limiting factor, and the excessive H₂O₂ produced by the GOx-catalyzed reaction diffused out of the microcapsule at a slow rate, resulting in its local accumulation in the COF microcapsule, which had an inhibitory effect on GOx, so that the measured enzyme activity at this time was lower; when HRP was in excess, GOx was the limiting factor, and the decrease in its content resulted in a gradual reduction in the amount of H₂O₂ produced, which in turn led to a reduction in the activity of the dual-enzyme system. The above results indicate that the bionic multienzyme cascades and the induced self-assembly morphology of COFs can be achieved simultaneously by using the Gemini surfactants.

Discussion

In summary, our biomimetic strategy not only replicates the structural hierarchy of natural biofilms but also introduces dynamic morphology control through enzyme-surfactant interactions. The model enzymes GOx and HRP can be rapidly and steadily immobilized in the COFs via this biomimetic strategy. We further revealed that the enzymes were also involved in the self-assembly process of COFs, which affects the morphology of COFs and bioactivities of themselves. The mechanism for the morphology regulation of enzymes@COF could be mainly attributed to the electrostatic interaction between the enzyme and the surfactant, which alters the self-assembly process. The interplay between enzyme charge, COF morphology (vesicle integrity, surface area, shell thickness), and synthesis parameters (oil-water ratio, surfactant type, monomer concentration) dictates tailoring COF morphology. In particular, the morphology plays a definitive role in the catalytic activity. 1) The vesicular structures are more advantageous for catalysis performance compared to lamellar structures, which suggests that the vesicular structure (*v*-TpPa-COF) offers a dual confinement effect for enzyme-substrate interactions, with its porous shell

protecting the enzyme and its internal cavity facilitating substrate diffusion. Conversely, the dense interlayer spacing of the lamellar structure (*l*-TpPa-COF) may impede substrate mass transfer, resulting in lower activity; 2) the worm-like or rod-like morphologies formed in the O/W system exhibit greater enzyme loading capacity, stability, and recyclability, which further demonstrate that co-assembly with COFs is an effective approach to immobilize enzymes; 3) in different loading systems, the O/W system provides superior stability and activity retention due to its robust vesicular morphology, while the W/O system shows moderate stability but is more prone to vesicle rupture. Higher enzyme loading can enhance activity but may also induce morphological changes and instability, necessitating optimization for maintaining desired morphology and maximizing performance; 4) additionally, shell thickness plays a crucial role, where the thinner shells facilitate better substrate access and thus comprise higher activity, and the excessively thin shells would lead to vesicle rupture and enzyme leakage, emphasizing the importance of the shell thickness to balance stability and activity. The immobilized enzyme by this strategy retained the high activity and stability, which is superior to other reported systems. Furthermore, the multienzyme cascade can be constructed by the self-assembled COFs. These rigid and stable organic framework vesicles may be an ideal substitute for liposomes for biological applications. The bioinspired, mild, and morphology-controlled one-pot method reported in this work provides a new and reliable strategy for enzyme immobilization.

Methods

Materials

Unless otherwise noted, all reagents and solvents were obtained from commercial sources and used directly without further purification. Deuterated solvents for NMR measurement were obtained from Aldrich. Distilled water was used in the experiments. Other chemicals used in this study were analytical reagent grade.

Synthetic procedures

General procedures for the synthesis of different morphological TpPa-COFs by screening surfactants in O/W system.

Various surfactants aqueous solutions (15 mL 1 mg mL⁻¹) were added into a 50 mL round-bottomed flask. The solution was stirred at 500 rpm, and Pa (24 mg, 0.225 mmol) was added. Subsequently, Tp (31.5 mg, 0.15 mmol) was ultrasonic dissolved in 3.5 mL dichloromethane and added to the above aqueous solution dropwise with an adding rate of 0.5 mL min⁻¹. The solution was further stirred at room temperature for 10 min. Upon the complete of the reaction, the solid was precipitated with 15 mL ethanol, and the solid red powder was obtained by filtration. The solid red powder was Soxhlet extracted with methanol and THF, respectively, for 12 h and vacuum dried at 100 °C.

General procedures for the synthesis of different morphological TpPa-COFs by screening surfactants in W/O system.

15 mL 1 mg mL⁻¹ surfactants mixed solution (o-DCB: CHCl₃ = 3:2) was added into a 50 mL round-bottomed flask, stirred at 500 rpm, and Pa (24 mg, 0.225 mmol) was added. 10 mg PVA was dissolved in 2 mL ultrapure water. Then, the mixture was added dropwise into the above solution. After that, Tp (31.5 mg, 0.15 mmol) was ultrasonic dissolved in 3 mL CHCl₃ and added to the above aqueous mixture by dropwise at a rate of 0.5 mL min⁻¹. The solution was stirred at room temperature for 10 min. Upon the complete of the reaction, the solid was precipitated with 15 mL ethanol, and the solid red powder was obtained by filtration. The solid red powder was Soxhlet extracted with methanol and THF, respectively, for 12 h and vacuum dried at 100 °C.

General procedures for enzyme immobilization in TpPa-COFs in O/W system

15 mL 1 mg mL⁻¹ surfactants aqueous solution was added into a 50 mL round-bottomed flask, stirred at 500 rpm. Then, 15 mg PVA was added

by stirring for 10 min and Pa (24 mg, 0.225 mmol) was added. After that, specified amount of enzyme (4, 8, 12, 16 and 20 mg) was dissolved in the above aqueous solution. Tp (31.5 mg, 0.15 mmol) was ultrasonic dissolved in 3.5 mL dichloromethane and added to the above aqueous mixture by dropwise at a rate of 0.5 mL min⁻¹. The solution was stirred at room temperature for 10 min. Upon the end of the reaction, centrifuge washing with deionized water for three times, freeze-dried to recover the red powder.

General procedures for enzyme immobilization in TpPa-COFs in W/O system

15 mL 1 mg mL⁻¹ surfactants mixed solution (o-DCB: CHCl₃ = 3:2) was added into a 50 mL round-bottomed flask, stirred at 500 rpm, and Pa (24 mg, 0.225 mmol) was added. 10 mg PVA was dissolved in 2 mL ultrapure water and specified amount of enzyme (4, 8, 12, 16 and 20 mg) was dissolved in the water. Then, the mixture was added dropwise into the above solution. After that, Tp (31.5 mg, 0.15 mmol) was ultrasonic dissolved in 3 mL CHCl₃ and added to the above aqueous mixture by dropwise at a rate of 0.5 mL min⁻¹. The solution was stirred at room temperature for 10 min. Upon the end of the reaction, the solution was washed with deionized water by centrifugation for three times, freeze-dried to recover the red powder.

Preparation of GOx&HRP@v-TpPa-COF(W/O)

15 mL 1 mg mL⁻¹ C₁₆₋₂₋₁₆ mixed solution (o-DCB: CHCl₃ = 3:2) was added into a 50 mL round-bottomed flask, stirred at 500 rpm, and Pa (24 mg, 0.225 mmol) was added. 10 mg PVA was dissolved in 2 mL ultrapure water and 4 mg with specified ratio of GOx&HRP (3:1, 2:1, 1:2, 1:3, 1:4, 1:5, 1:6) was dissolved in the water, and then the mixture was added dropwise into the above organic solution. After that Tp (31.5 mg, 0.15 mmol) was ultrasonic dissolved in 3 mL CHCl₃ and added to the above aqueous mixture by dropwise at a rate of 0.5 mL min⁻¹. The solution was stirred at room temperature for 10 min. Upon the end of the reaction, centrifuge washing with deionized water for three times, freeze-dried to recover the red powder.

Characterization. ¹H NMR spectra were recorded on a JEOL (JNM-ECZ400S/L1) 400 MHz spectrometer, where chemical shifts (δ in ppm) were determined with a residual proton of the solvent as standard. Solid-state ¹³C CP/MAS NMR measurement was recorded using a JNM-ECZ600R spectrometer. The Powder X-ray diffraction (PXRD) measurements were performed using X-ray diffraction (D8 Advance, Bruker), which was equipped with Cu Kα radiation (λ = 1.54056 Å) at the scattering angle 2θ between from 2θ = 3.0 to 35°. The Fourier transform infrared spectra (FT-IR) were recorded with a Mattson Alpha-Centauri spectrometer (Nicolet iS50, Thermo Scientific) in the range 4000–400 cm⁻¹. Nitrogen sorption isotherms were measured at 77 K with a Micrometer ASAP 2020 and BSD-16 analyzer. Before measurement, the samples were degassed in a vacuum at 120 °C for more than 12 h. Specific surface areas and pore volume were calculated by using the Brunauer-Emmett-Teller (BET) method. Thermogravimetric analysis (TGA) (STA 449F5, Perkin Elmer Instruments) with a temperature interval between 35 and 800 °C. Scanning electron microscopy (SEM) images were obtained with a MAIA3 LMH. TESCAN Transmission electron microscopy (TEM) images of the samples were characterized by transmission electron microscope (Talos L120C G2). UV-vis absorption spectra were obtained in solid state on a Lambda 950, PerkinElmer. The confocal laser scanning microscopy images were collected on Leica TCS SP8 STED 3X under an excitation of 633 nm and 405 nm. Dynamic light scattering and Zeta potential were obtained with Zetasizer Nano ZSE.

Data availability

The datasets generated and analyzed during the current study are available in the repository. Additional data are available from the

corresponding author upon request. Source data are present. Source data are provided with this paper.

References

- Bornscheuer, U. T. et al. Engineering the third wave of biocatalysis. *Nature* **485**, 185–194 (2012).
- Wu, S., Snajdrova, R., Moore, J. C., Baldenius, K. & Bornscheuer, U. T. Biocatalysis: Enzymatic Synthesis for Industrial Applications. *Angew. Chem. Int. Ed.* **60**, 88–119 (2021).
- Maghraby, Y. R., El-Shabasy, R. M., Ibrahim, A. H. & Azzazy, H. M. E.-S. Enzyme Immobilization Technologies and Industrial Applications. *ACS Omega* **8**, 5184–5196 (2023).
- Bilal, M. & Iqbal, H. M. N. Chemical, physical, and biological coordination: An interplay between materials and enzymes as potential platforms for immobilization. *Coord. Chem. Rev.* **388**, 1–23 (2019).
- Walde, P. & Ichikawa, S. Enzymes inside lipid vesicles: preparation, reactivity and applications. *Biomolecular Eng.* **18**, 143–177 (2001).
- Jin, C. et al. Enzyme Immobilization in Porphyrinic Covalent Organic Frameworks for Photoenzymatic Asymmetric Catalysis. *ACS Catal.* **12**, 8259–8268 (2022).
- Zhao, Z. et al. Engineering Olefin-Linked Covalent Organic Frameworks for Photoenzymatic Reduction of CO₂. *Angew. Chem. Int. Ed.* **61**, e202200261 (2022).
- Ran, L. et al. Covalent Organic Frameworks Based Photoenzymatic Nano-reactor for Asymmetric Dynamic Kinetic Resolution of Secondary Amines. *Angew. Chem. Int. Ed.* **63**, e202319732 (2024).
- Gao, R. et al. Ionic Liquid-Mediated Dynamic Polymerization for Facile Aqueous-Phase Synthesis of Enzyme-Covalent Organic Framework Biocatalysts. *Angew. Chem. Int. Ed.* **63**, e202319876 (2024).
- Huang, S. et al. Hydrogen-Bonded Supramolecular Nanotrap Enabling the Interfacial Activation of Hosted Enzymes. *J. Am. Chem. Soc.* **146**, 1967–1976 (2024).
- Wang, C. & Liao, K. Recent Advances in Emerging Metal- and Covalent-Organic Frameworks for Enzyme Encapsulation. *ACS Appl. Mater. Interfaces* **13**, 56752–56776 (2021).
- Feng, J., Huang, Q.-Y., Zhang, C., Ramakrishna, S. & Dong, Y.-B. Review of covalent organic frameworks for enzyme immobilization: Strategies, applications, and prospects. *Int. J. Biol. Macromol.* **248**, 125729 (2023).
- Kandambeth, S. et al. Self-templated chemically stable hollow spherical covalent organic framework. *Nat. Commun.* **6**, 6786 (2015).
- Sun, Q. et al. Pore Environment Control and Enhanced Performance of Enzymes Infiltrated in Covalent Organic Frameworks. *J. Am. Chem. Soc.* **140**, 984–992 (2018).
- Sun, Q., Aguila, B., Lan, P. C. & Ma, S. Tuning Pore Heterogeneity in Covalent Organic Frameworks for Enhanced Enzyme Accessibility and Resistance against Denaturants. *Adv. Mater.* **31**, 1900008 (2019).
- Xing, C. et al. Enhancing Enzyme Activity by the Modulation of Covalent Interactions in the Confined Channels of Covalent Organic Frameworks. *Angew. Chem. Int. Ed.* **61**, e202201378 (2022).
- Yang, X. et al. Fabrication of a hierarchical nanoreactor based on COFs for cascade enzyme catalysis. *Chem. Commun.* **58**, 3933–3936 (2022).
- Tang, Y. et al. Fabrication of hollow covalent-organic framework microspheres via emulsion-interfacial strategy to enhance laccase immobilization for tetracycline degradation. *Chem. Eng. J.* **421**, 129743 (2021).
- Zhang, S. et al. Covalent Organic Frameworks with Chirality Enriched by Biomolecules for Efficient Chiral Separation. *Angew. Chem. Int. Ed.* **57**, 16754–16759 (2018).

20. Liang, J. et al. Insight into Bioactivity of In-situ Trapped Enzyme-Covalent-Organic Frameworks. *Angew. Chem. Int. Ed.* **62**, e202303001 (2023).
21. Zheng, Y. et al. Green and Scalable Fabrication of High-Performance Biocatalysts Using Covalent Organic Frameworks as Enzyme Carriers. *Angew. Chem. Int. Ed.* **61**, e202208744 (2022).
22. Fan, X., Zhai, S., Xue, S. & Zhi, L. Enzyme Immobilization using Covalent Organic Frameworks: From Synthetic Strategy to COFs Functional Role. *ACS Appl. Mater. Interfaces* **16**, 40371–40390 (2024).
23. Li, M. et al. Fabricating Covalent Organic Framework Capsules with Commodious Microenvironment for Enzymes. *J. Am. Chem. Soc.* **142**, 6675–6681 (2020).
24. Wang, M. et al. Visual naked-eye detection of SARS-CoV-2 RNA based on covalent organic framework capsules. *Chem. Eng. J.* **429**, 132332 (2022).
25. Meyfour, A. et al. The quest of cell surface markers for stem cell therapy. *Cell. Mol. Life Sci.* **78**, 469 (2021).
26. Menger, F. M. & Keiper, J. S. Gemini Surfactants. *Angew. Chem. Int. Ed.* **39**, 1906–1920 (2000).
27. Kandambeth, S. et al. Construction of Crystalline 2D Covalent Organic Frameworks with Remarkable Chemical (Acid/Base) Stability via a Combined Reversible and Irreversible Route. *J. Am. Chem. Soc.* **134**, 19524–19527 (2012).
28. Zhang, J., Cheng, C., Guan, L., Jiang, H.-L. & Jin, S. Rapid Synthesis of Covalent Organic Frameworks with a Controlled Morphology: An Emulsion Polymerization Approach via the Phase Transfer Catalysis Mechanism. *J. Am. Chem. Soc.* **145**, 21974–21982 (2023).
29. Lombardo, D., Calandra, P., Pasqua, L. & Magazù, S. Self-Assembly of Organic Nanomaterials and Biomaterials: The Bottom-Up Approach for Functional Nanostructures Formation and Advanced Applications. *Materials* **13**, 1048 (2020).
30. Israelachvili, J. N., Mitchell, D. J. & Ninham, B. W. Theory of self-assembly of hydrocarbon amphiphiles into micelles and bilayers. *J. Chem. Soc., Faraday Trans. 2* **72**, 1525–1568 (1976).
31. Bhardwaj, P., Kamil, M. & Panda, M. Surfactant-polymer interaction: effect of hydroxypropylmethyl cellulose on the surface and solution properties of gemini surfactants. *Colloid Polym. Sci.* **296**, 1879–1889 (2018).
32. Song, B. & Cho, C.-W. Applying polyvinyl alcohol to the preparation of various nanoparticles. *J. Pharm. Investig.* **54**, 249–266 (2024).
33. Chen, L. et al. Imparting multi-functionality to covalent organic framework nanoparticles by the dual-ligand assistant encapsulation strategy. *Nat. Commun.* **12**, 4556 (2021).
34. Zhang, Y. et al. Harnessing Self-Repairing and Crystallization Processes for Effective Enzyme Encapsulation in Covalent Organic Frameworks. *J. Am. Chem. Soc.* **145**, 13469–13475 (2023).
35. Rajput, S. M. et al. Formation of hydrotropic drug/gemini surfactant based catanionic vesicles as efficient nano drug delivery vehicles. *Colloid Interface Sci. Commun.* **37**, 100273 (2020).
36. Rodrigues, R. C., Ortiz, C., Berenguer-Murcia, Á, Torres, R. & Fernández-Lafuente, R. Modifying enzyme activity and selectivity by immobilization. *Chem. Soc. Rev.* **42**, 6290–6307 (2013).
37. Wu, X., Ge, J., Yang, C., Hou, M. & Liu, Z. Facile synthesis of multiple enzyme-containing metal-organic frameworks in a biomolecule-friendly environment. *Chem. Commun.* **51**, 13408–13411 (2015).
38. Wohlfahrt, G. et al. 1.8 and 1.9 Å resolution structures of the resolution structures of the *Penicillium amagasakiense* and *Aspergillus niger* glucose oxidases as a basis for modelling substrate complexes. *Acta Crystallogr. D. Biol. Crystallogr.* **55**, 969–977 (1999).
39. Berglund, G. I. et al. The catalytic pathway of horseradish peroxidase at high resolution. *Nature* **417**, 463–468 (2002).

Acknowledgements

We acknowledge the financial support from National Natural Science Foundation of China (no. 22275143, S.J.), Shaanxi Provincial Outstanding Youth Science Fund (no. 2025JC-JCQN 002, S.J.), Key Project of Natural Science Basic Research Program of Shaanxi (no. 2023JC-XJ-14, S.J.) and Qinchuangyuan High Level Innovation and Entrepreneurship Talent Project (no. QCYRCXM-2022-23, S.J.). We also appreciate for the technical support by the Analysis and Testing Center of the Xi'an Jiaotong University in the characterizations of each materials. We thanks for the support from the Xi'an Key Laboratory of C1 Compound Bioconversion Tenology.

Author contributions

S.J. conceived the project and supervised the experiments. J. Z. conducted the syntheses and designed the experiments, structure analyses and characterizations for all the samples and interpreted the data. J.L. conducted the nitrogen sorption experiment. L.Z. provided suggestions on the application of bioactivities performance. Y.L. conducted the SEM experiment. J.Z. and S.J. wrote the manuscript and all the authors reviewed it.

Competing interests

The authors declare no competing interests.

Additional information

Supplementary information The online version contains supplementary material available at <https://doi.org/10.1038/s41467-025-60719-z>.

Correspondence and requests for materials should be addressed to Shangbin Jin.

Peer review information *Nature Communications* thanks Zhong-Xing Zhao, and the other, anonymous, reviewer(s) for their contribution to the peer review of this work. A peer review file is available.

Reprints and permissions information is available at <http://www.nature.com/reprints>

Publisher's note Springer Nature remains neutral with regard to jurisdictional claims in published maps and institutional affiliations.

Open Access This article is licensed under a Creative Commons Attribution-NonCommercial-NoDerivatives 4.0 International License, which permits any non-commercial use, sharing, distribution and reproduction in any medium or format, as long as you give appropriate credit to the original author(s) and the source, provide a link to the Creative Commons licence, and indicate if you modified the licensed material. You do not have permission under this licence to share adapted material derived from this article or parts of it. The images or other third party material in this article are included in the article's Creative Commons licence, unless indicated otherwise in a credit line to the material. If material is not included in the article's Creative Commons licence and your intended use is not permitted by statutory regulation or exceeds the permitted use, you will need to obtain permission directly from the copyright holder. To view a copy of this licence, visit <http://creativecommons.org/licenses/by-nc-nd/4.0/>.

© The Author(s) 2025